Lab on a Chip

PAPER

View Article Online
View Journal

Cite this: DOI: 10.1039/d6lc00211k

Centrifugal microfluidic automation of the protein aggregation capture workflow for robust mass spectrometry-based proteomics

Michelle Hinrichs, †[ab] Johanna Wallner, †[cd] Johanna Thiery,[ef] Carolin Kleber,[b] Manuel Metzger,[ab] Stephan A. Sieber,[c] Tobias Hutzenlaub,[ab] Oliver Schilling,[e] Nils Paust,[ab] Hannes Hahne,[d] Jan Muntel[d] and Jan-Niklas Klatt *[ab]

Proteomic sample preparation for liquid chromatography-tandem mass spectrometry (LC-MS/MS) is increasingly addressed by automated approaches. However, in clinical settings for precision medicine, where a limited number of samples must be processed in a standardized and reproducible manner with minimal user interaction, fully automized workflows remain scarce. Here, we present the AutoPAC-disk, a centrifugal microfluidic implementation of a protein aggregation capture (PAC) sample preparation workflow for bottom-up proteomics that automates all necessary steps for on-bead proteolysis including on-disk pre-storage of buffers. Comparative evaluation of the AutoPAC-disk using HEK293 cell lysates against a manual reference workflow and a semi-automated robotic PAC implementation showed 50% and 37% more peptide identifications and 23% and 10% more protein group identifications, respectively, while maintaining high quantitative reproducibility as reflected by protein-group intensity coeffincients of variation (CVs) below 10%. Additional analysis demonstrated that the AutoPAC-disk primarily increased identifications of low-abundance proteins without introducing method specific physicochemical bias. The AutoPAC-disk was subsequently evaluated using patient-derived formalin-fixed paraffin-embedded (FFPE) prostate tumor tissue. The AutoPAC-disk yielded 8% more peptide identifications and 10% more protein groups than the manual workflow, with protein-group intensity CVs below 7% for both methods. Together, these results demonstrate that centrifugal microfluidic automation with on-disk buffer pre-storage can substantially simplify proteomic sample preparation, minimize user interaction and lower operational barriers for personnel with limited experience in proteomic sample preparation, providing a promising strategy for clinical and translational proteomics in the field of precision medicine.

Received 5th March 2026,
Accepted 23rd May 2026

DOI: 10.1039/d6lc00211k

rsc.li/loc

Introduction

Precision medicine aims to improve therapeutic efficacy while minimizing adverse effects, and is gaining traction in clinical applications, including but not limited to oncology.[1] Comprehensive molecular characterization of patient-derived samples is fundamental to such approaches and is typically achieved through the integration of various – omics technologies.[1,2] While genomics-based stratification methods are already well established in clinical and translational research, mass-spectrometry (MS)-based proteomics remains comparatively underrepresented, despite growing evidence that proteomic information can substantially enhance diagnostic and therapeutic decision-making.[3,4] This added clinical value is increasingly reflected in emerging applications, including the integration of MS-based proteomics into molecular tumor boards[5] and the recent recommendation by the College of American Pathologists to include MS-based proteomic typing of amyloidosis.[6] Despite these emerging clinical applications and the ability of MS-based proteomics to capture dynamic, patient-specific protein expression and signaling states, its widespread implementation in routine clinical workflows remains limited.[7]

[a] Hahn-Schickard, Georges-Koehler-Allee 304, 79110 Freiburg, Germany. E-mail: niklas.klatt@hahn-schickard.de
[b] Laboratory for MEMS Applications, IMTEK-Department of Microsystems Engineering, University of Freiburg, Georges-Koehler-Allee 304, 79110 Freiburg, Germany
[c] Chair of Organic Chemistry II, Center of Functional Protein Assemblies (CPA), TUM School of Natural Sciences, Technical University of Munich, Ernst-Otto-Fischer Strasse 8, 85748 Garching, Germany
[d] OmicScouts, a Momentum Biotechnologies Company, Lise-Meitner-Strasse 30, 85354 Freising, Germany
[e] Institute for Surgical Pathology, Medical Center, University of Freiburg, Breisacher Strasse 115a, 79106 Freiburg, Germany
[f] Faculty of Biology, University of Freiburg, Schaenzlestrasse 1, 79104 Freiburg, Germany
† Contributed equally.

Among proteomic strategies, bottom-up proteomics has become the most commonly adopted approach. It enables comprehensive characterization of patient-specific proteomes by liquid chromatography-tandem mass spectrometry (LC-MS/MS) analysis of proteolytically generated peptides,[8] which are directly detected and quantified to provide largely unbiased insights.[9,10] Reliable MS-based proteomics critically depends on robust and reproducible sample preparation, and recent methodological developments have led to numerous optimized protocols.[11,12] One widely adopted approach is single-pot solid-phase enhanced sample preparation (SP3),[13,14] which operates *via* protein aggregation capture (PAC).[15,16] In PAC workflows, proteins are precipitated and immobilized on beads, allowing efficient removal of MS-incompatible contaminants and subsequent on-bead digestion for peptide analysis, while maintaining reproducibility and enabling robust preparation of complex samples.[16,17] While this approach provides higher sample purity than in-solution workflows, it is more complex, as bead handling requires numerous pipetting steps and therefore depends on highly skilled personnel for robust and reliable operation. To address the lack of reproducibility, several semi-automated PAC workflow solutions are available to simplify the complex and labor-intensive sample preparation, including implementations on the KingFisher (Thermo Fisher Scientific)[17] and the BRAVO liquid handling platform (Agilent).[18] Although these systems automate the majority of bead handling steps and reduce manual workload, they remain complex to operate and still rely on highly trained personnel, as critical steps such as organic solvent handling and interaction with sophisticated software interfaces are not fully automated. Moreover, such platforms are primarily designed for high-throughput applications and entail substantial investment costs. Our experience shows that emerging MS-based proteomics applications in pathology diagnostics (*e.g.*, for the molecular tumor board or amyloidosis typing) result in a single-digit number of samples per day. We anticipate the requirement for an automated sample processing setup that addresses (a) a small number of samples per day, (b) alleviates the need for major instrumentation investment, and (c) minimizes the need for extensive user training by reducing user interaction through pre-loaded reagents and workflow integration.

To address these requirements, microfluidic technologies are well-suited, as they enable miniaturization, process integration, and automation of complex laboratory workflows with lower sample numbers. Within this field, centrifugal microfluidics is particularly well-suited for automated and standardized proteomic sample preparation assays, as liquid transport is driven by centrifugal force, requiring minimal instrumentation while enabling robust processes and user-friendly operation.[19] During rotation, centrifugal microfluidics generates a gravitational field that exceeds 1 g by several orders of magnitude, causing body forces to dominate over capillary and other surface-related forces. This enables robust fluid handling with reliable bead bed retention and liquid–solid phase separation, promotes the removal of entrapped air through density differences, and reduces susceptibility to surface-induced failure modes. Due to these technological features, centrifugal microfluidic systems have already been successfully applied to automate a range of laboratory workflows, including highly sensitive, multiplexed qPCR for minimal residual disease monitoring,[20] sample preparation for next-generation sequencing[21] and proteomics, especially in-solution digestion[22] and desalting *via* solid phase extraction.[23] These centrifugal microfluidic implementations for proteomic sample preparation address isolated workflow steps and are not compatible with PAC-based strategies. The approach based on in-solution digestion[22] is unsuitable for samples requiring high concentrations of detergents and chaotropes, as the design does not implement bead-based washing and handling steps essential for PAC workflows. Similarly, the implementation focused on desalting *via* solid-phase extraction[23] cannot be transferred to on-bead digestion, as the design neither supports reagent pre-storage nor stable multi-hour incubation of the enzymatic digestion mixture within the bead bed required for efficient proteolysis.

Yet, a completely automated centrifugal system for MS-based proteomic sample preparation with pre-stored reagents and user-friendly operation, designed for straightforward integration into routine clinical workflows, has not yet been realized. In contrast to centrifugal microfluidic approaches, other microfluidic strategies used in proteomics have predominantly focused on processing extremely small sample amounts. In particular, droplet-based platforms such as NanoPOTS or digital microfluidic approaches have been reported in the literature.[24–27] These approaches are highly effective for ultra-low-input applications but typically rely on complex actuation principles, such as electrowetting-on-dielectric control of discrete droplets or the precise dispensing of nanoliter-scale volumes, which require specialized instrumentation. In addition, the integration of pre-stored reagents is challenging in these systems, such that external reagent handling and user interaction remain necessary, limiting their suitability for the low-intervention, time-sensitive workflows required in clinical applications.

In this work, we demonstrate the centrifugal microfluidic implementation of a PAC workflow by conceptually redesigning the assay to enable robust microfluidic operation, including reliable bead handling and on-disk reagent pre-storage to minimize user interaction. The resulting AutoPAC-disk was evaluated using HEK293 cell lysates and benchmarked against a manual reference PAC workflow and a semi-automated robotic implementation to assess comparative performance. In addition, the AutoPAC-disk was exemplarily applied to clinically relevant formalin-fixed paraffin-embedded (FFPE) prostate tumor lysates.

Experimental

Design and fabrication of the microfluidic AutoPAC-disk

The design of the microfluidic layout was carried out in SolidWorks (Dassault Systèmes, France) and supported by network-based simulations performed in MATLAB Simulink Simscape (MathWorks, USA), as described previously.[28] The fabrication of the microfluidic disks followed an established protocol, starting with milling (KERN Microtechnik, Germany) the negative design in PMMA (Evonik, Germany). Subsequently, a positive Elastosil RT-607 PDMS (Wacker Chemie, Germany) master was cast. The actual disks were produced in foil technology by micro-thermoforming employing co-extruded 6013/8007 cyclic olefin copolymer (COC) foils (TekniPlex, USA) and a modified hot embossing machine (Jenoptik, Germany). Sealing of the disks was achieved by pressure-assisted thermal bonding.[29] Pre-storage of washing and binding buffer was realized by manually filling stick packs with 250 µL of 80% ethanol and 180 µL of 100% ethanol (Roth, 5054.3), followed by manual sealing with a sealing clamp (HAWO, Germany). Stick packs were manually inserted into the sealed disk by opening the respective chambers and subsequent sealing using adhesive films (9795T, 3M Center, USA). For final assembly, a custom made PMMA (Evonik, Germany) insulation frame was glued onto the disk using double sided adhesive tape (Tesa, Germany).

PAC-based workflows and sample preparation for nLC-MS/MS

nLC-MS/MS samples were prepared using three different PAC workflows as illustrated in Table 1. The performance of the microfluidic disk was evaluated against a manual protocol and a semi-automated protocol using a KingFisher Apex robot (ThermoFisher Scientific, 5 400 930). Owing to the experimental setup, the AutoPAC-disk experiments with HEK293 lysate were conducted on two consecutive days. For the evaluation experiments, 20 µg denatured, reduced, and alkylated HEK293 lysate SI_methods: M1) (0.4 µg μL^{-1}) was used for all workflows.

Carboxylated-modified SpeedBeads (Cytiva, GE65152105050250, GE45152105050250) at a protein:bead ratio of 1 : 10 w/w were used in the manual and KingFisher workflow. Beads were pre-washed three times with ddH_2O and resuspended in their working volume prior to use. Proteins were precipitated by adding ethanol to a final concentration of 70% ethanol (v/v) and incubation for binding (10 minutes at 1000 rpm, room temperature, in the manual workflow; 30 minutes on the KingFisher workflow). Beads were then captured magnetically (rack for manual; instrument magnets for KingFisher), and the supernatant was removed and discarded. In the manual protocol, beads were washed three times with 200 µL of 80% ethanol (Roth, 5054.3), followed by a brief air-drying step (5 minutes, open tube) to remove residual ethanol. In the KingFisher workflow, beads were washed three times with 250 µL of 80% ethanol (Roth, 9065.2). For on-bead digestion, beads were resuspended in ammonium bicarbonate buffer (manual: 100 mM ABC (Sigma-Aldrich, 09830-500G), pH 8.0; KingFisher: 50 mM ABC (Roth, T817)), and sequencing-grade trypsin (Promega, V5111) was added at a protein : enzyme ratio of 1 : 25 (w/w). Digestion

Table 1 Overview of evaluated proteomic sample preparation workflows and their main processing steps. The microfluidic, bead-packed digestion device is hereafter referred to as the AutoPAC-disk (AutoPAC-disk workflow). A semi-automated magnetic bead-based protocol implemented on the KingFisher Apex robot is further denoted as KingFisher workflow. The manual reference PAC workflow, hereafter referred to as the manual workflow, was used as the primary comparator due to its conceptual similarity to the AutoPAC-disk workflow

Workflows	AutoPAC	KingFisher	Manual
		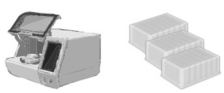	
Beads	Protein to bead ratio: 1 : 1 (w/v) Bead size: 30 µm	Protein to bead ratio: 1 : 10 (w/w) Bead size: 1 µm	Protein to bead ratio: 1 : 10 (w/w) Bead size: 1 µm
Binding	Buffer: 100% EtOH Time: 10 min	Buffer: 100% EtOH Time: 30 min	Buffer: 100% EtOH Time: 10 min
Washing	Buffer: 80% EtOH Volume: 1 × 250 µL	Buffer: 80% EtOH Volume: 3 × 250 µL	Buffer: 80% EtOH Volume: 3 × 200 µL
Digestion	Digestion volume and time: 14 µL, 4 hours Protein to enzyme ratio: 1 : 25 trypsin in 100 mM ABC (pH 8)	Digestion volume and time: 50 µL, 16 hours Protein to enzyme ratio: 1 : 25 trypsin in 50 mM ABC (pH 8)	Digestion volume and time: 104 µL, 4 hours Protein to enzyme ratio: 1 : 25 trypsin in 100 mM ABC (pH 8)
Post-processing	Acidification: add TFA 1% (v/v) TFA final Sample treatment: centrifugation drying in vacuum concentrator	Acidification: second bead elution with TFA combine with sample 1% (v/v) TFA final Sample treatment: stage-tipping	Acidification: add TFA 1% (v/v) TFA final Sample treatment: centrifugation drying in vacuum concentrator

proceeded at 37 °C (manual: 4 hours at 1000 rpm on a thermoshaker; KingFisher: overnight at 650 rpm on a thermoshaker). In the manual workflow, the reaction was stopped by acidification to a final concentration of 1% TFA (Merck, 1082180050). In the KingFisher workflow, beads were additionally washed with 2% TFA (Th. Geyer, 044630. AP) to recover residual peptides, and both eluates were combined with a final concentration of 1% TFA.

As an initial step for preparing the AutoPAC-disk, 20 μL of the 25% PureCube (Cube Biotech, 50 201) bead suspension was washed twice with 1 mL PBS (Gibco, 20 012-019) and once with 1 mL ddH_2O. After washing, the beads were resuspended in 80 μL ddH_2O for loading into the bead inlet. Subsequently, 50 μL of reduced and alkylated protein lysate was pipetted into the sample inlet, followed by a digestion mix consisting of 10 μL 100 mM ammonium bicarbonate buffer (pH 8) (Sigma-Aldrich, 09830-500G) and 4 μL sequencing grade modified trypsin with a 1 : 25 (protein : enzyme) w/w ratio (Promega, V5111) into the respective inlet. The AutoPAC-disk was processed on the Rhonda player[21,23,30] developed by Hahn Schickard, Dialunox and Spindiag. All experiments were performed on a test rig equipped with a stroboscopic set-up (Hamilton, Germany) to monitor liquid movement in real time. Once the disk was inserted into the Rhonda player, a pre-defined protocol (SI_results: R1, Fig. 3) that controls the rotational frequency and the temperature of the ten different heating zones of the player was executed to perform the automated workflow. After completion of the protocol, the peptide solution was collected from the disk, and the reaction was subsequently quenched by acidifying the solution to a final concentration of 1% TFA (Merck, 1082180050).

Following completion of sample preparation workflows, post-processing was performed to ensure UHPLC-MS/MS compatibility. KingFisher samples were cleaned *via* the stage-tip protocol[31] to eliminate bead carryover. Acidified supernatants from AutoPAC-disk and manual samples were transferred to fresh tubes and centrifuged (full speed, 10 minutes). The resulting supernatant was again transferred to a fresh tube, followed by drying in a vacuum concentrator (Eppendorf) at 45 °C and storage at −80 °C.

nLC-MS/MS setup and acquisition

Proteomic samples were analyzed using an Orbitrap Exploris 480 mass spectrometer (Thermo Fisher Scientific) with a Vanquish Neo UHPLC-system (Thermo Fisher Scientific) equipped with a trap cartridge (Pepmap 100 C18 5 μm 0.3 × 5 mM, Thermo Katalog Dreieich, 174500) and an analytical column (Aurora Frontier XT, IonOpticks, AUR3-60075C18-XT). Peptides were separated on the analytical column using a gradient ranging from 4% to 32% buffer B (0.1% FA (Roth, 1EHK.1), 5% dimethylsulfoxide (Pierce, 85 190) in HPLC-MS grade acetonitrile (Chemsolute, 2697)) in buffer A (0.1% FA (Roth, 1EHK.1), 5% dimethylsulfoxide (Pierce, 85 190) in HPLC-MS grade water (Chemsolute, 455)). For each sample, 600 ng peptide were injected, dissolved in 0.1% FA with 2% acetonitrile (Chemsolute, 2697).

For peptide separation 100 minutes gradients were used and MS/MS spectra were recorded with data-independent acquisition (DIA) (MS1 orbitrap resolution 60 000, MS1 scan range 400–1000, MS1 RF lens 40, MS1 normalized AGC target 300%, MS1 maximum injection time 20 ms, MS2 mode tMS2, MS2 orbitrap resolution 30 000, MS2 scan range 200–1600 *m*/*z*, HCD collision energy 27%, MS2 normalized AGC target 2000%, MS2 maximum injection time 54 ms, DIA window coverage 400–1000 *m*/*z* with 30 windows with 12.15 *m*/*z* and 10 windows with 25.5 *m*/*z*, 0.5 *m*/*z* overlap).

nLC-MS/MS data analysis

DIA raw files were converted to *.mzML* using MSConvertGui (peak Picking vendor msLevel = 1−, zeroSamples removeExtra 1−) (ProteoWizard[32]). *mzML* files were searched using FragPipe v23.1.[33] Only replicates were searched together. Decoys and contaminants were added to a human FASTA, based on the SwissProt entries from January 2024, containing protein isoforms. MSFragger (version 4.3 (ref. 33)) was used for identification (protein digestion: stricttrypsin; variable modification: oxidation of methionine and protein N-terminal acetylation; fixed modification: carbamidomethylation of cysteines). Quantification was performed using DIA-NN v1.8.1 (ref. 34) without normalization (–no-norm).

Proteomic data processing and visualization

The report.tsv, report.pr_matrix.tsv and report.pg_matrix.tsv MSFragger output files were used. All files were processed in R[35] and RStudio.[36] Data was visualized using ggplot2.[37] Physicochemical properties of peptides and protein groups were analyzed using peptides.[38] All analyses were restricted to peptides and protein groups that were identified and quantified. Coefficients of variation (CVs) were calculated on protein group level including all identified and quantified protein groups. Beforehand, LFQ intensities were normalized on the overall median.

Results and discussion

Design concept and assay adaptations for microfluidic implementation

To enable a robust microfluidic implementation of PAC with minimal user interaction, key assay parameters were adapted prior to integration into the centrifugal microfluidic platform. First, 30 μm PureCube beads (CubeBiotech, 50 201) were selected, as their size enables reliable bead retention and packing through purely geometric confinement. Previous scanning electron microscope-based analysis of the bead size distribution showed measurable size variation around the nominal diameter and was considered in defining a retention structure height of 13 μm. This dimension was selected to ensure stable retention of the packed bead bed without frits or additional retaining elements, thereby simplifying

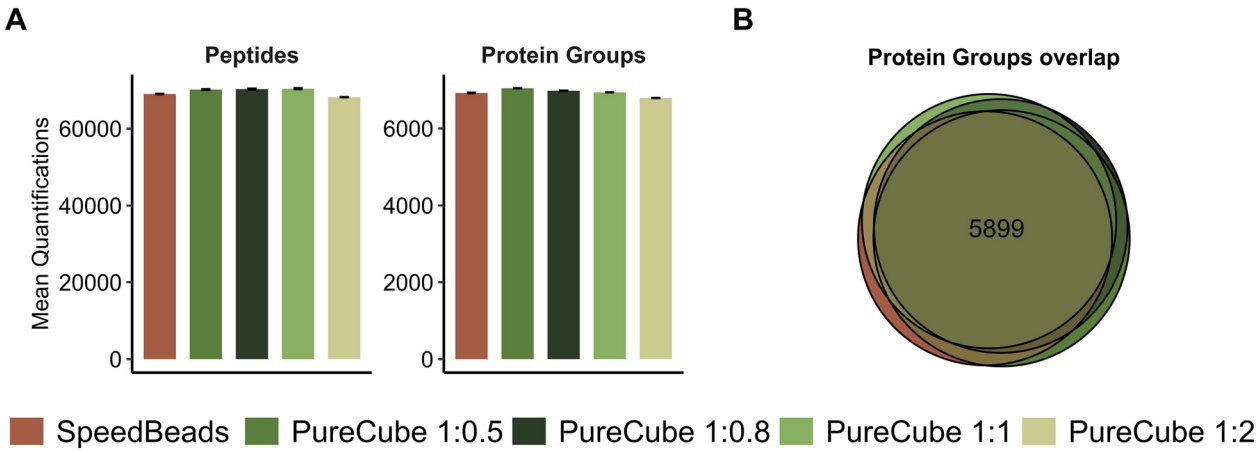

Fig. 1 Comparison and protein-to-bead ratio of PureCube magnetic beads to SpeedBeads for the protein aggregation capture (PAC) workflow. (A) Mean of quantified peptides (left) and protein groups (right) (SpeedBeads (protein : beads 1 : 10, w/w) (orange) and PureCube beads (protein : bead slurry 1 : 0.5, 1 : 0.8, 1 : 1, 1 : 2 w/v) (green scales) (n = 3, error bars: standard deviation). (B) Venn diagrams show the protein group overlaps between the different beads and bead titrations (n = 3; PureCube 1 : 2 excluded).

fabrication. Second, solvent and reagent conditions were streamlined for microfluidic compatibility. Ethanol was chosen as a unified precipitation and washing solvent to reduce toxicity and variability while maintaining performance. Additionally, the feasibility of reagent pre-storage and the impact of solvent concentration on protein capture efficiency were systematically evaluated. Detailed methods and materials for the assay adaptation experiments are provided in the SI (SI_methods: M2 and M3).

PureCube beads (Cube Biotech) were tested in varying protein-to-bead ratios (1 : 0.5, 1 : 0.8, 1 : 1, and 1 : 2, w/v, referring to the 25% stock bead suspension) against 1 μm SpeedBeads (Cytiva), which are commonly used in PAC protocols (1 : 10, w/w)[14,16,39] on the KingFisher Apex. The corresponding bead volume was estimated by calculating the number of 30 μm beads required to approximate the total surface area of the reference SpeedBead condition and converting this to the required volume of 25% PureCube suspension. This resulted in an approximate protein-to-bead ratio of 1 : 1 (w/v). To account for potential deviations from this theoretical estimate and to ensure robust method optimization, a broader range (1 : 0.5 to 1 : 2, w/v) was subsequently investigated experimentally, enabling systematic evaluation of bead quantities.

More than 70 000 peptides and around 7000 protein groups were quantified with 0.5, 0.8 and 1 μL PureCube bead slurry per 1 μg protein lysate (0.5 μL: peptides: 70 193, protein groups: 7050, 0.8 μL: peptides: 70 325, protein groups: 6984; 1 μL: peptides: 70426, protein groups: 6943), matching the performance of SpeedBeads (peptides: 69 045, protein groups: 6928) (Fig. 1(A)). High (2 μL per 1 μg protein) PureCube bead inputs resulted in a slightly lower number of quantified peptides and protein groups (peptides: 68 210, protein groups: 6796) (Fig. 1(A)). Peptide and protein level analysis of physicochemical properties, such as peptide hydrophobicity, molecular weight, and isoelectric point, gave comparable results across all tested conditions, indicating no systematic bias or loss due to those properties (SI_results: Fig. 1). Furthermore, a 71.2% overlap of protein groups between SpeedBeads and the PureCube input amounts with highest identifications (PureCube 1 : 0.5, 1 : 0.8, and 1 : 1 w/v) supports the robustness and reproducibility of the PAC workflow performed with the larger PureCube beads (Fig. 1(B)).

To simplify and unify the solvent handling, acetonitrile and ethanol precipitation was tested with a final organic solvent concentration from 30 to 70% and compared against an in-house developed standard workflow (precipitation with 70% ethanol, 1st and 2nd wash with 100% acetonitrile, 3rd wash with 80% ethanol) (Fig. 2(A)). At 30%, acetonitrile and ethanol yielded substantially fewer protein groups and peptides compared to the standard workflow, with acetonitrile showing the largest loss (standard workflow: 7073 protein groups, 66 948 peptides; 30% acetonitrile: 3052 protein groups, 18 774 peptides; 30% ethanol: 3604 protein groups, 23 239 peptides). Increasing the concentration to 50% improved recovery, approaching—but not fully reaching—the standard workflow (50% acetonitrile: 6582 protein groups, 62 971 peptides; 50% ethanol: 6691 protein groups, 63 277 peptides). Full coverage was restored at 70% solvent for both acetonitrile and ethanol (70% acetonitrile: 6779 protein groups, 66 450 peptides; 70% ethanol: 7060 protein groups, 68 108 peptides). Workflow robustness followed the same pattern: low solvent concentrations resulted in high variability (30% ethanol: 17.2%; 30% acetonitrile: 11.5%), while 50% and 70% precipitations achieved reproducibility comparable to the standard workflow, with only marginal increases in CV at the highest concentrations (50% ethanol: 2.7%; 50% acetonitrile: 3.8%, 70% ethanol: 3.1%, 70% acetonitrile 4.8%, standard 3.2%) (Fig. 2(B)). Regarding the proteomic coverage, samples that were precipitated using only 30% organic solvent showed fewer low-abundant protein

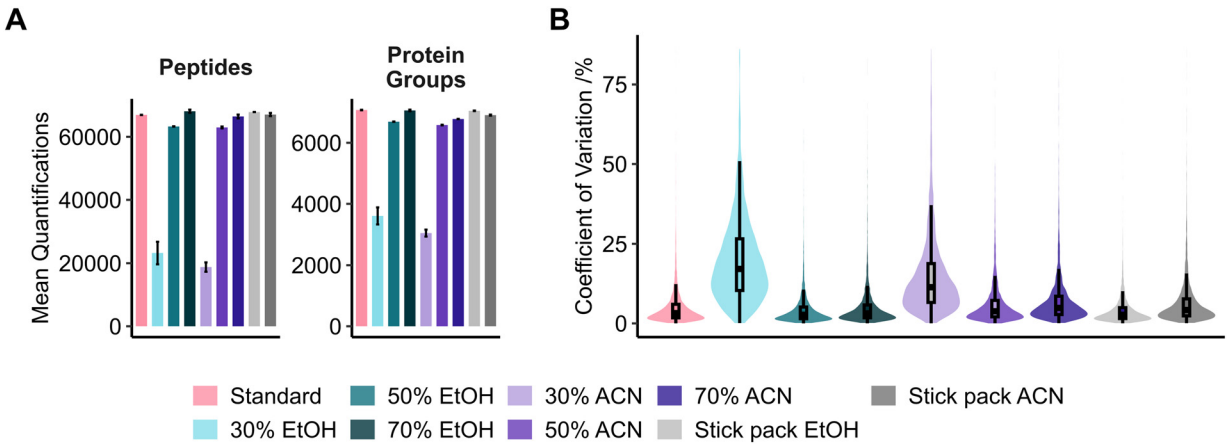

Fig. 2 Comparison of different organic solvents for the protein aggregation capture (PAC) workflow. (A) Mean of quantified peptides (left) and protein groups (right) for the standard workflow (precipitation with 70% ethanol; washes two times 80% ethanol, one time 100% acetonitrile) with different solvent concentrations of ethanol and acetonitrile during the binding step, and for workflows using ethanol or acetonitrile stick packs compatible with microfluidic pre-storage. 30%/50%/70% ethanol protein precipitation on beads (three times 80% ethanol washes) and 30%/50%/70% acetonitrile protein precipitation on beads (three times 100% acetonitrile washes) (n = 3, error bars: standard deviation). All conditions were tested using the KingFisher Apex (pink: standard control; bright grey: stick pack with ethanol; dark grey: stick pack with acetonitrile; blue range: 30%, 50%, 70% ethanol precipitation; purple range: 30%, 50%, 70% acetonitrile precipitation). (B) Coefficients of variation (CV) of median normalized protein group quantities for three different protein lysate inputs (color coding identical to (A)). Boxplots show the median (thick line), 25th and 75th percentiles (hinges), the whiskers extend to ±1.5 times the inter-quartile range.

groups, while all other samples covered a broad range of protein group intensities (SI_results: Fig. 2). Furthermore, no relevant differences in physicochemical properties between ethanol- and acetonitrile-based workflows were found (SI_results: Fig. 2). Our results demonstrated that a final ethanol concentration of at least 70% (v/v) is required for optimal protein binding, exceeding the 50% recommended by literature.[14,17] The use of 80% ethanol for washing, consistent with literature, was comparable with the standard workflow (Fig. 2).[15,17,39]

To enable a fully automated PAC-based microfluidic workflow with minimal user interaction, organic solvents must be pre-stored on the disk. In centrifugal microfluidics, liquid reagent pre-storage in sealed stick packs is an established concept for genomic applications. Therefore, we evaluated the feasibility of pre-storing organic solvents on the AutoPAC-disk for proteomic sample preparation by using prestored solvents in a manual setup. Using sealed stick packs, we applied single-solvent workflows (70% solvent for precipitation; 100% acetonitrile or 80% ethanol for washing). Performance matched that of fresh solvents, including numbers of quantified peptides and protein groups and overall workflow robustness (peptide: 67 861 (ethanol); 67 061 (acetonitrile); protein groups: 7048 (ethanol), 6909 (acetonitrile); CV: 2.7% (ethanol), 4.2% (acetonitrile) (Fig. 2(A) and (B), grey bars)).

Collectively, the evaluated assay adaptations, namely the use of larger beads, ethanol as a unified solvent and reagent pre-storage, enabled a high number of quantified peptides and protein groups, delivering the basis for a robust centrifugal microfluidic implementation.

Microfluidic AutoPAC-disk

The AutoPAC-disk (Fig. 3) is based on centrifugal microfluidics, where liquid transport is driven primarily by centrifugal force.[19] Automated liquid handling within the disk is achieved by combining centrifugal actuation with thermopneumatic pumping induced by localized heating.[40–42] Processing of the AutoPAC-disk in a fully automated manner is performed by the Rhonda player (Fig. 3).[21,23,30] Each disk comprises two structures for simultaneous processing of two samples, with buffers pre-stored in stick packs that automatically release the liquids under centrifugation[43] to minimize user interaction (Fig. 3).

The main steps of the automated sample preparation are outlined in Fig. 4(B–D). The complete microfluidic protocol, including all rotational frequencies and temperatures of the depicted heating zones, is detailed in the SI (SI_results: Fig. 3).

In a first step, the user adds 50 µL sample, 14 µL digestion mix (1:25 trypsin in 100 mM ABC), and 80 µL bead suspension into the inlet chambers of the AutoPAC-disk (Chambers 2, 4, and 6) (Fig. 4(A)). The bead suspension is centrifuged in the bead column chamber with a total volume of 260 µL, which tapers to a 13 µm retention zone, where intact 30 µm beads are packed to form a bead bed that enables protein precipitation and on-bead digestion with individually adaptable incubation times. More detailed information about the bead column chamber and the bead bed can be found in the SI (SI_results; Fig. 4). In contrast to earlier work[23] the AutoPAC-disk implements a PAC-based on-bead digestion workflow with substantially different requirements regarding bead handling, incubation, and

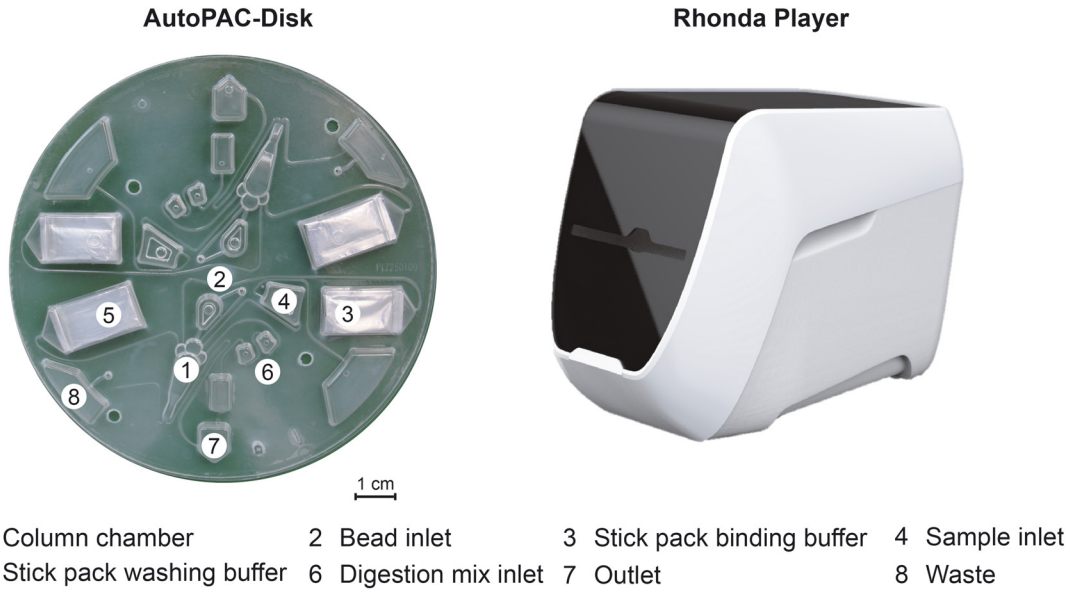

Fig. 3 Photograph of the AutoPAC-disk (left), which consists of two mirrored fluidics, one of them is numbered. Both fluidic structures contain the aluminum stick packs for pre-storage. The processing device, Rhonda player, is displayed as an illustration on the right side.

waste management. Accordingly, the downstream switching concept was fundamentally redesigned. Instead of routing liquids *via* intermediate collection chambers followed by thermopneumatic transfer, supernatant volumes exceeding 30 μL are directed directly to waste through an integrated downstream fluidic switch (Fig. 4(A)). This enables efficient removal of all used buffers while reducing dependence on local heating for transport into the waste chamber. This is due to the radial position of the meniscus (r_1) in the bead column chamber, which lies radially inward of the radial position of the volume siphon crest (r_2) for liquid volumes greater than 30 μL, as illustrated in Fig. 4(B). For the binding step, pre-stored 100% ethanol is first released from the stick pack by a combination of elevated rotational frequency and localized heating at heating zone 1 (Fig. 4(A)). Reducing the rotational frequency then enables transfer of ethanol to the bead column chamber *via* thermopneumatic pumping.[41,42] After transfer of the binding buffer, the sample is transferred by thermopneumatic valving into the bead column chamber.[42] Binding conditions achieving at least a final ethanol concentration of 70% can be maintained up to a sample volume of 70 μL; in this proof of principle study, a 50 μL sample volume is used. The binding buffer and sample are subsequently mixed *via* shake mode[44] at moderate frequencies in order to keep the pre-mature transfer into the waste as low as possible. For the subsequent washing step, the stick pack containing 80% ethanol is opened as already described for the binding buffer stick pack by the combination of centrifugation and thermopneumatic pumping (Fig. 4(C)).[41,42] The 250 μL washing buffer is perfused through the bead bed and is also routed to the waste chamber. Digestion commences thereafter, initiated by thermopneumatic valving transfer[42] of 14 μL digestion mix from chamber 6 to the bead column (Fig. 4(A)). This 14 μL digestion mix volume fully wets the bead bed without priming the volume siphon leading to the waste chamber. The design of the AutoPAC-disk permits arbitrarily long incubation times through customized protocols, as routing the digestion medium to the outlet chamber needs active priming of the outlet siphon. In this proof-of-concept study, digestion is performed at 37 °C for 4 hours within the bead column chamber. After digestion is completed, the sample is transferred into the outlet chamber by priming the outlet siphon *via* thermopneumatic pressure (Fig. 4(D)). Heating zone 3 (Fig. 4(A)) is heated to displace the air from the outlet chamber at low rotational speeds. After the air has been displaced, the temperature is reduced to ambient conditions. The contracting air volume generates a pressure lower than the ambient pressure that propels priming of the inverted outlet siphon. Once primed, the eluate can be transferred into the outlet chamber by centrifugal force.

Comparative performance of the AutoPAC-disk, the manual, and KingFisher PAC workflows

To evaluate the performance of the newly developed AutoPAC-disk, aliquots of 20 μg HEK293 lysate (n = 4) were processed with the AutoPAC-disk workflow, a manual PAC protocol, and a PAC workflow implemented on the KingFisher Apex robot. Digestion time was set to 4 hours for the AutoPAC-disk and manual workflows and 16 hours for the KingFisher setup. Identification depth, coefficient of variation, and sequence coverage are summarized in Fig. 5. Samples processed with the AutoPAC-disk yielded 79 436 peptides, representing a 50% increase over the manual workflow (53 088) and a 37% increase over the KingFisher workflow (57 832). At the protein group level, the AutoPAC-disk quantified 7643 protein groups, compared to 6962

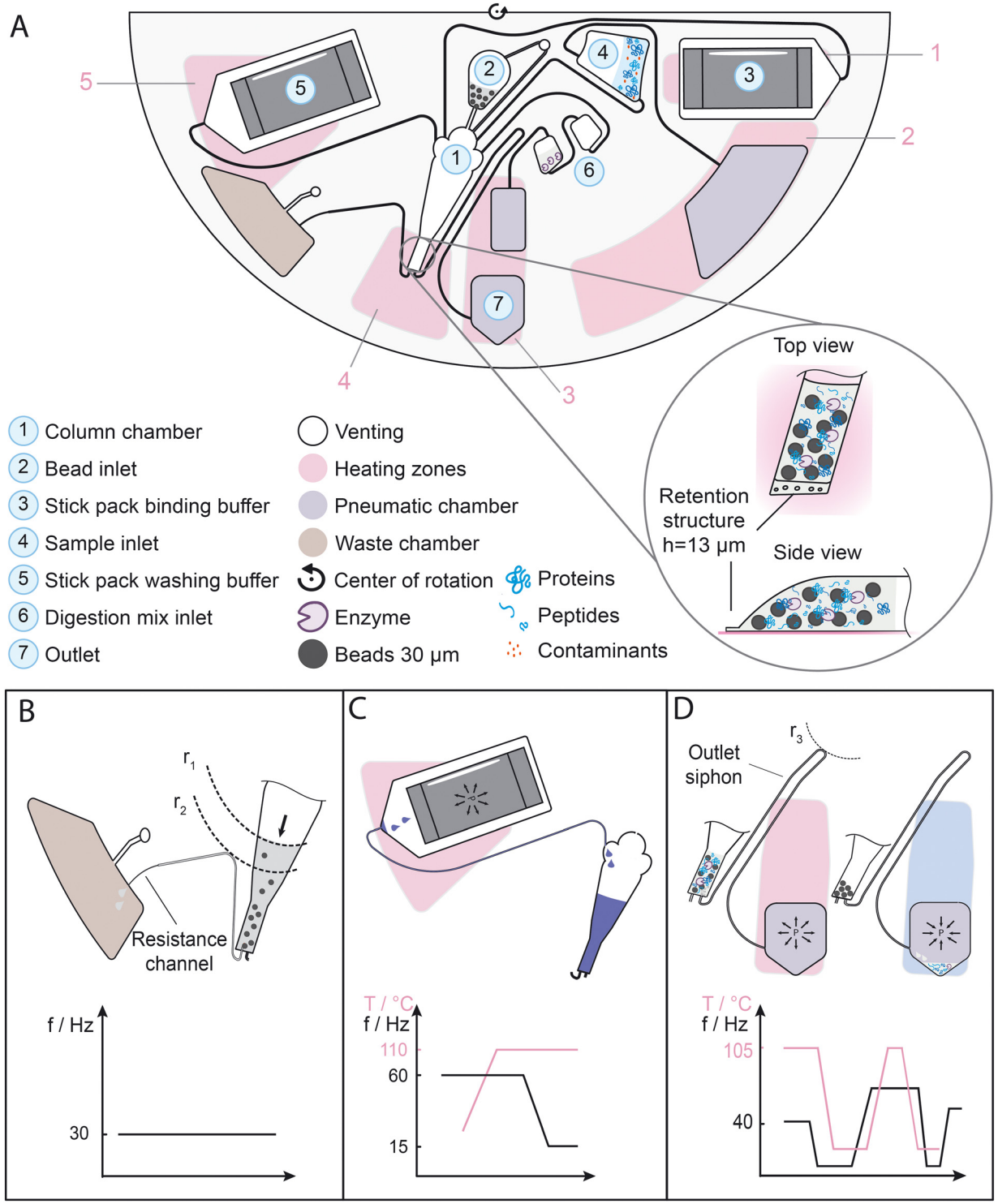

Fig. 4 Centrifugal microfluidic concept of the AutoPAC-disk. (A) A schematic illustration of the AutoPAC-disk layout, showing magnification of the bead column chamber. Heating zones of the turntable on the Rhonda player are depicted in light pink and numbered. (B) Microfluidic layout of the bead column chamber, including the binding step protocol and the transfer of the supernatant through the volume siphon. (C) Section of the microfluidic layout displaying the opening of the washing stick pack using a combination of high rotational speed and temperature for opening and subsequent lower rotational speed for pumping. (D) Microfluidic layout of the bead column chamber, showing the protocol for transferring the sample to the outlet chamber *via* thermopneumatic pumping. To denote cooling, the heating zone is depicted in blue.

(KingFisher) and 6223 (manual), corresponding to a 10% and 23% increase, respectively (Fig. 5(A)). To assess reproducibility, coefficients of variation (CVs) of protein intensities were calculated for each workflow. Fig. 5(B) shows

an excellent protein-level CV well below 10% for all workflows. The AutoPAC-disk exhibits slightly higher variability (7.5%) compared to the KingFisher (3.2%) and manual workflows (4.1%). This increase is consistent with the higher number of low-abundance proteins identified using the AutoPAC-disk, which are inherently more variable. Nevertheless, the observed CVs remain within the range reported for established proteomic workflows.[17,45] Across workflows, 34 350 peptides and 5025 protein groups were commonly quantified (Fig. 5(C)). The AutoPAC-disk workflow exhibited greater peptide overlap with both the KingFisher (11501) and manual workflows (14 711) than the overlap between the manual and KingFisher workflows alone (1018). The increased number of peptide quantifications achieved with the AutoPAC-disk is reflected by 21 916 peptides quantified exclusively with this approach. A similar trend was observed at the protein group level, with 1168 protein groups quantified exclusively with the AutoPAC-disk, compared to 766 protein groups quantified exclusively with the KingFisher workflow and 414 with the manual approach. Sequence coverage of quantified protein groups is shown in Fig. 5(D), demonstrating that the higher number of peptide quantifications obtained with the AutoPAC-Disk results in increased sequence coverage of quantified protein groups. Assessment of digestion efficiency and peptide length (SI_results: Fig. 5) confirmed that the AutoPAC-disk and manual workflow, both performed at identical digestion conditions, exhibited comparable cleavage efficiency. These findings exclude semi-tryptic contributions as the cause of the increased peptide and protein quantification rates observed for the microfluidic approach. Furthermore, no systematic differences in the physicochemical properties of quantified peptides and proteins were detected between all three workflows (SI_results: Fig. 6).

To systematically assess how the observed performance differences manifest across the dataset, we performed a deeper comparative analysis of abundance distributions (Fig. 6). When analyzing the protein group rank depending on their intensity, AutoPAC-disk samples yield a broader rank distribution, reflecting the increased number of protein group quantifications, whereas proteins quantified using the KingFisher workflow spanned a similar overall intensity

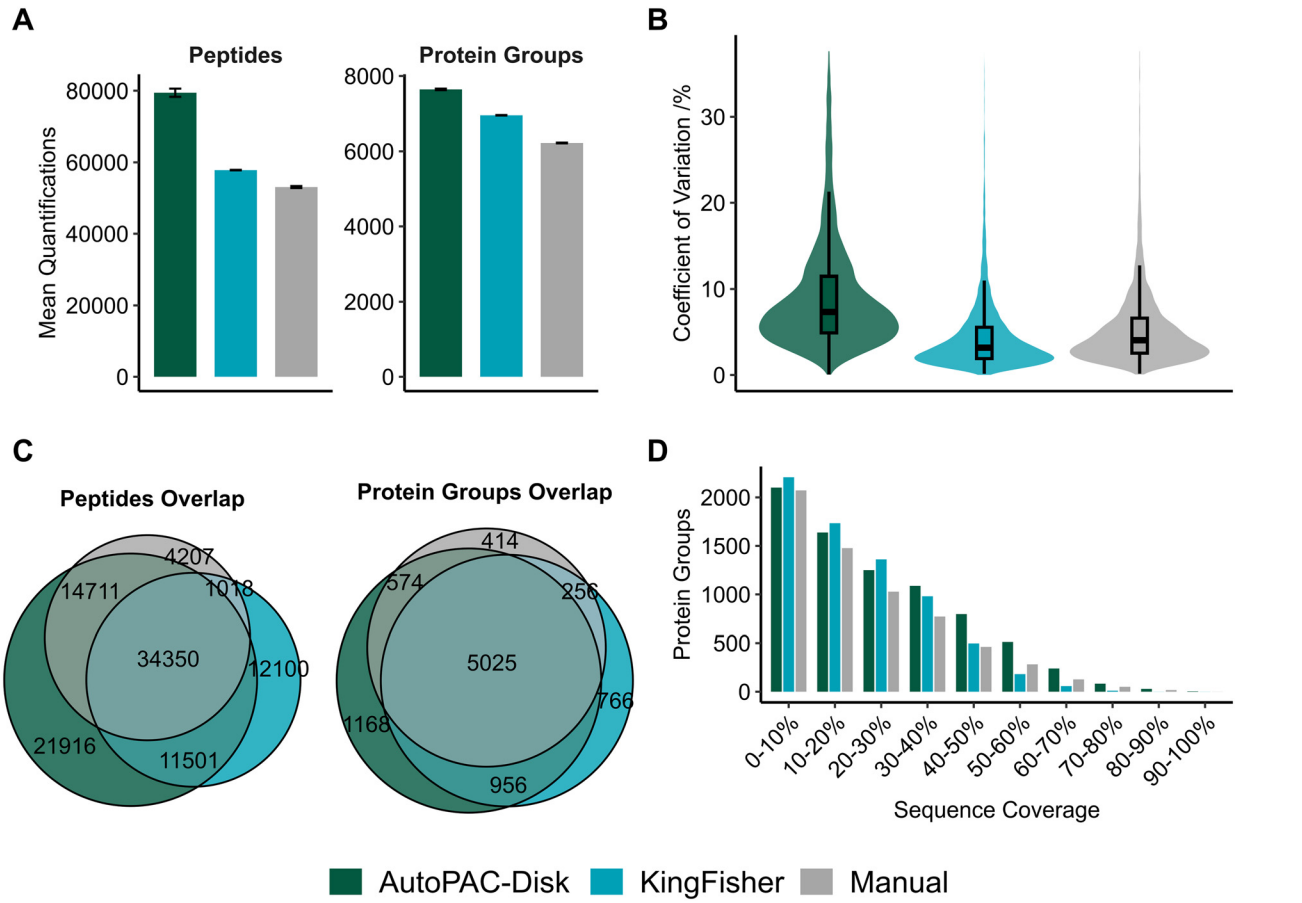

Fig. 5 (A) Mean of quantified peptides (left) and protein groups (right) for the AutoPAC-disk (green), KingFisher (blue), and manual (grey) PAC workflow (n = 4, error bars: standard deviation). (B) Violin plots show the coefficient of variation (CV) of median normalized protein group quantities for the three workflows. The thick line represents the median, the upper and lower hinges of the boxplot represent the 25th and 75th percentiles, the whiskers extend to ±1.5 times the inter-quartile range, colored as described in (A). (C) Venn diagrams show peptide (left) and protein group (right) overlaps between the three different PAC workflows, colored as described in (A). (D) Sequence coverage of unique proteins for AutoPAC-disk, KingFisher, and manual workflow, colored as described in (A).

range as those quantified with the other approaches, but extended further toward lower-abundance proteins (Fig. 6(A)). The manual workflow showed an intermediate intensity distribution, with fewer protein group quantifications overall, resulting in a leftward shift of the intensity-rank profile. The peptide rank plots demonstrated analogous performance; the results are presented in the SI (SI_results: Fig. 7). A global protein group rank, representing only exclusively found protein groups, indicates that workflow-specific exclusive proteins span the full abundance range, with the lowest-abundance proteins being exclusively detected by the KingFisher workflow (Fig. 6(B)).

To comprehensively evaluate how quantified protein groups and peptides obtained with the three workflows are distributed across the abundance range, global abundance ranks were divided into percentiles. For each percentile, the relative fractions of quantifications that were exclusive to a single workflow, shared between any two workflows, or common to all three workflows were calculated with respect to all quantifications within that percentile. Based on these calculations, heatmaps (Fig. 6(C) and (D)) were generated. Each column of the heatmaps corresponds to one area of the Venn diagrams, which are depicted in Fig. 5(C). At the peptide level (Fig. 6(C)), analysis of the lowest-abundance percentile (90–100%) showed that 20.4% of peptides were quantified exclusively by the KingFisher workflow, whereas 17.3% were quantified exclusively by the AutoPAC-disk and 18.3% by the manual workflow. With increasing abundance percentiles, the fraction of workflow-exclusive peptide quantifications decreased continuously across all three approaches. While differences between the workflows were detectable, they remained comparatively small across percentiles. In parallel, the proportion of peptides commonly quantified by all three workflows increased steadily with increasing abundance. Peptides quantified by at least two workflows showed comparatively stable contributions across abundance percentiles, except for the highest-abundance percentile, where their relative fraction declined.

At the protein group level (Fig. 6(D)), differences between the workflows were more pronounced, especially at low abundances. In the lowest-abundance percentile (90–100%), 29.2% of the proteins were quantified exclusively by the AutoPAC-disk, compared to 24.9% for the KingFisher workflow and 14.9% for the manual approach. As protein abundance increased, the proportion of workflow-exclusive protein quantifications decreased for all approaches, while the fraction of commonly quantified proteins increased. Mixed subsets, comprising proteins quantified by two workflows, showed less clear trends, except for the proteins that were quantified by the AutoPAC-disk and the KingFisher. This subset featured the same pattern as the exclusive subsets with decreasing percentage for higher abundance percentiles. Overall, this analysis demonstrates that protein groups exclusively quantified by the AutoPAC-disk account for a substantial fraction of low-abundance protein quantifications.

This analysis is complemented by Fig. 6(E) and (F), which show the normalized cumulative peptide- and protein group-level quantifications for each workflow plotted as a function of global abundance rank. These plots graphically illustrate whether the quantifications obtained by each workflow are predominantly located in the low- or high-abundance range. At the peptide level (Fig. 6(E)), the KingFisher workflow shows a larger fraction of its quantifications in the high-abundance peptide range compared to the AutoPAC-disk and the manual workflow. In the upper third of the rank spectrum, this trend reverses. Overall, the observed differences between workflows remain relatively modest. As shown in Fig. 6(F), protein quantifications obtained with the AutoPAC-disk are shifted toward the low-abundance range, as indicated by a slower accumulation of protein quantifications at low ranks. In contrast, protein quantifications from the manual workflow increase almost linearly across the rank spectrum, indicating that a larger fraction of its total quantifications is already reached at any given rank. The KingFisher workflow exhibits an intermediate behavior between these two profiles.

Finally, Fig. 7 presents an analysis of peptides and proteins exclusively identified by each workflow. Panels (A)–(C) show the density distributions for the physicochemical properties of these exclusive peptides, including hydrophobicity, molecular weight, and isoelectric point. Differences in the hydrophobicity of exclusive peptides and proteins were minimal, with intensity median values of −0.5 ± 0.8 (peptides) and −0.4 ± 0.4 (proteins) for the AutoPAC-disk workflow, −0.3 ± 0.9 (peptides) and −0.4 ± 0.4 (proteins) for the KingFisher workflow, and −0.7 ± 0.8 (peptides) and −0.4 ± 0.3 (proteins) for the manual workflow (Fig. 7(A)). The molecular weight distributions were comparable across methods, with a median of 1395.4 ± 1.4 Da (AutoPAC-disk), 1250.3 ± 1.3 Da (KingFisher) and 1259.3 ± 1.4 Da (manual) for exclusive peptides in all workflows and median values of 51621.3 ± 2.2 Da (KingFisher), 50 425.9 ± 2.3 Da (manual) and 56865.8 ± 2.2 Da (AutoPAC-disk) for exclusive protein groups (Fig. 7(B)). Density distribution of the isoelectric point (pI) of the exclusive peptides showed three characteristic peaks for each method, with the median values being at 6.2 ± 2.2 (AutoPAC-disk), 6.3 ± 2.2 (KingFisher), and 7.5 ± 2.5 (manual) (Fig. 7(C)). All three workflows displayed similar median intensities for exclusive peptides in the density plot, 325 682.4 ± 2.8 (AutoPAC-disk), 348 610.1 ± 3.3 (KingFisher), and 333 186.1 ± 2.9 (manual) with a corresponding distribution in the lower intensity range, whereas common peptides showed a shift to higher intensity values (median 1 033 298.6 ± 3.8) (Fig. 7(D)). In agreement with the previous analyses, the density distribution of the KingFisher workflow indicates an increased relative contribution of exclusive peptide quantifications at low intensities. Fig. 7(E) shows the corresponding absolute counts of exclusively quantified

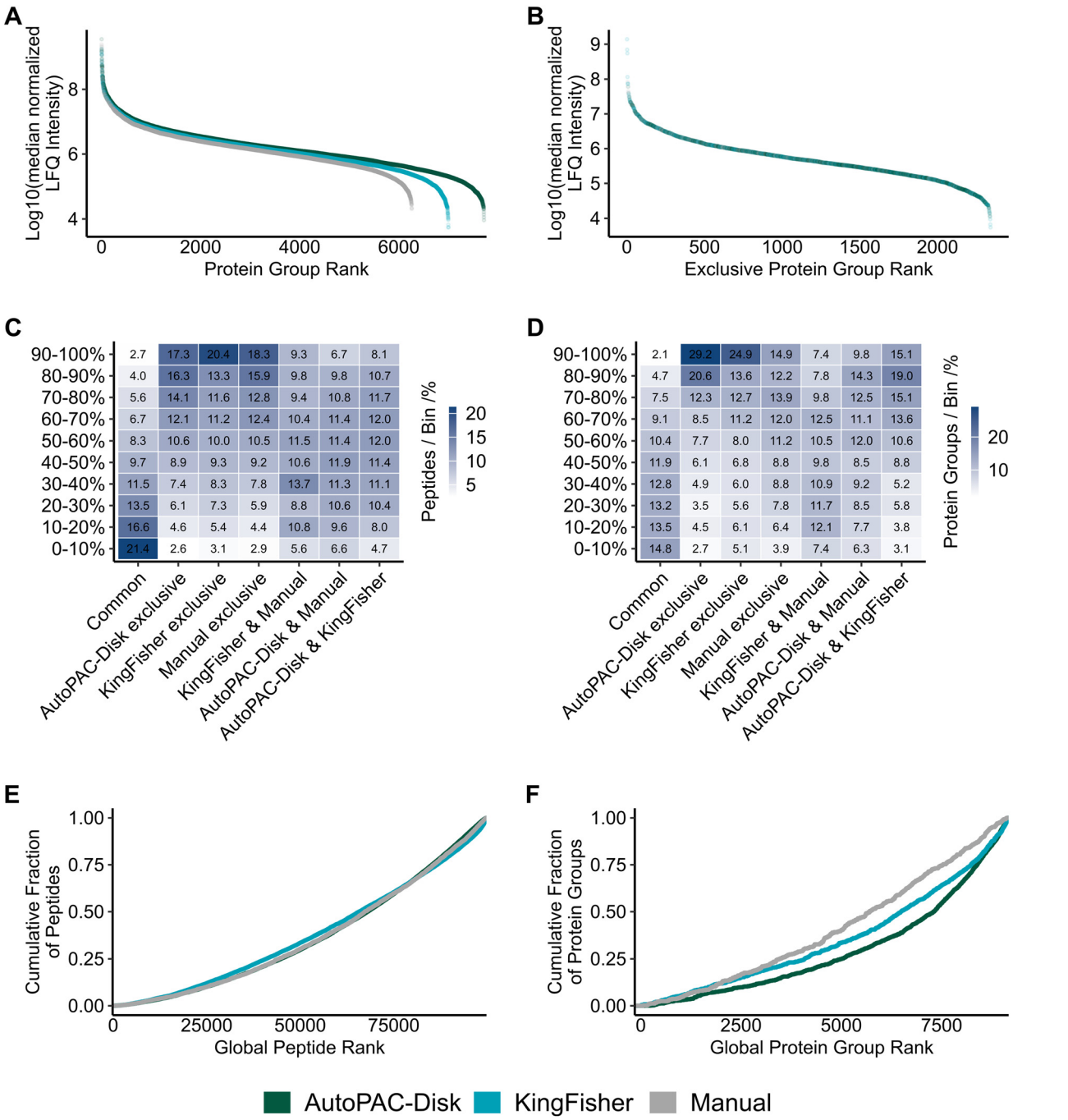

Fig. 6 Analysis of the proteomic range covered in samples processed with the AutoPAC-disk. (A) Protein group rank plot with log10 normalized protein intensity plotted over rank for each workflow separately (AutoPAC-disk: green, KingFisher: blue, manual: grey). (B) Global protein group rank with $\log_{10}$ normalized protein group intensity plotted for exclusively identified protein groups, color-coded as described in (A). (C) Heatmap showing a percentile-binned rank distribution of peptide quantifications across the three workflows. (D) Heatmap showing a percentile-binned rank distribution of protein group quantifications across the three workflows. Each column of the heatmaps corresponds to one area of the Venn diagram. (E) Global peptide rank plot for cumulative fraction of peptides colored as described in (A). (F) Global protein group rank plot for cumulative fraction of protein groups colored as described in (A).

peptides. The KingFisher and AutoPAC-disk workflows yield higher counts across the full intensity range, whereas the relative distribution of the subset remains largely comparable. For exclusive protein groups, the density plots indicated that the AutoPAC-disk workflow was shifted toward lower intensities (median value 355 214.6 ± 3.9), the KingFisher workflow occupied an intermediate range (median value 511 196.5 ± 4.9), and the manual workflow was shifted toward higher intensities (median value 712 379.3 ± 3.7), all remaining below the intensity range

observed for common protein groups (median value 1 770 876.7 ± 4.1) (Fig. 7(D)). In the corresponding count plots, the AutoPAC-disk yielded the highest numbers of exclusive proteins overall, with a shift to lower protein intensities compared to the other two workflows (Fig. 7(E)).

The comparative analysis across workflows excludes several explanations for the increased peptide and protein identification rates observed with the AutoPAC-disk. Neither physicochemical property distributions of identified peptides, digestion efficiency (SI results, Fig. 5), nor bead chemistry (Fig. 1) showed systematic differences, ruling out altered selectivity or incomplete proteolysis as contributing factors. Instead, the AutoPAC-disk consistently yielded a higher number of low-abundance peptide and protein identifications, indicating improved overall recovery rather than physicochemical bias. These observations suggest that differences in bead handling represent the most plausible explanation for the improved performance of the AutoPAC-disk. In contrast to the comparator workflows, the AutoPAC-disk confines beads in a stationary, geometrically defined microcolumn throughout processing. The KingFisher robot repeatedly transfers beads magnetically between wells, whereas manual protocols rely on intermittent magnetic immobilization and resuspension steps.

We hypothesize that the stationary bead bed format reduces bead loss during transfer steps and minimizes variability associated with repeated resuspension. In addition, maintaining proteins aggregated on a confined bead bed may reduce mechanical disturbance of bead–protein assemblies during processing, thereby improving overall analyte recovery.

A slightly higher proportion of fully cleaved peptides was also observed for the AutoPAC-disk compared to the manual 4 hours reference digest (47% *vs.* 44%; SI results, Fig. 5), suggesting that the stationary format may additionally provide favorable local conditions for enzymatic digestion. However, this effect is unlikely to be the primary driver of the increased identification numbers.

Collectively, these findings indicate that the mode of bead handling is the central technical distinction between the workflows and likely contributes to the superior analytical performance of the AutoPAC-disk.

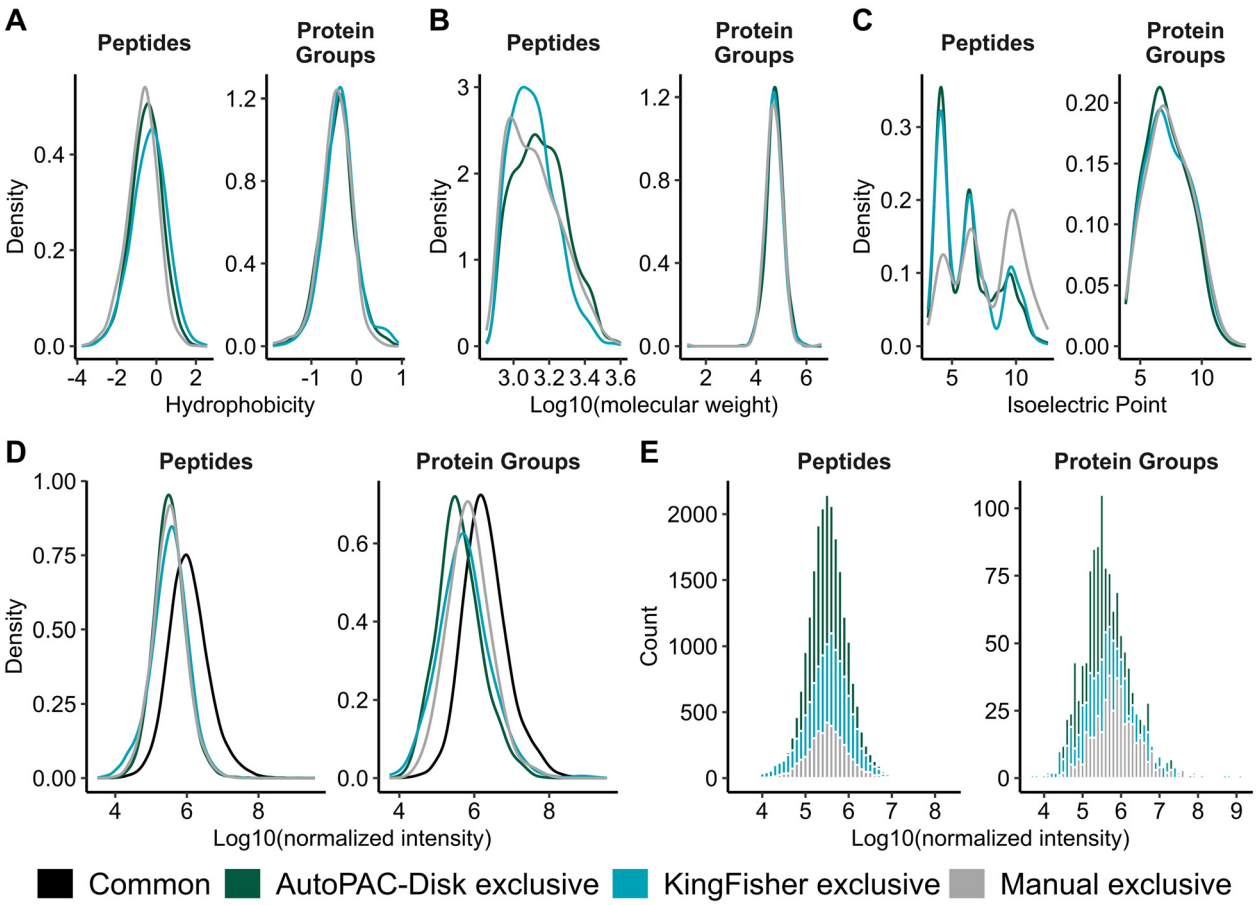

Fig. 7 Density distributions of physicochemical properties for identified peptides (left panels) and their exclusive protein groups (right panels) for n = 4 commons in black, AutoPAC-disk in green, KingFisher in blue, and manual in grey: (A) hydrophobicity, (B) molecular weight, (C) isoelectric point, and (D) $\log_{10}$-transformed normalized intensities. (E) Distributions of quantification counts as a function of $\log_{10}$-transformed normalized intensities for peptides (left) and protein groups (right).

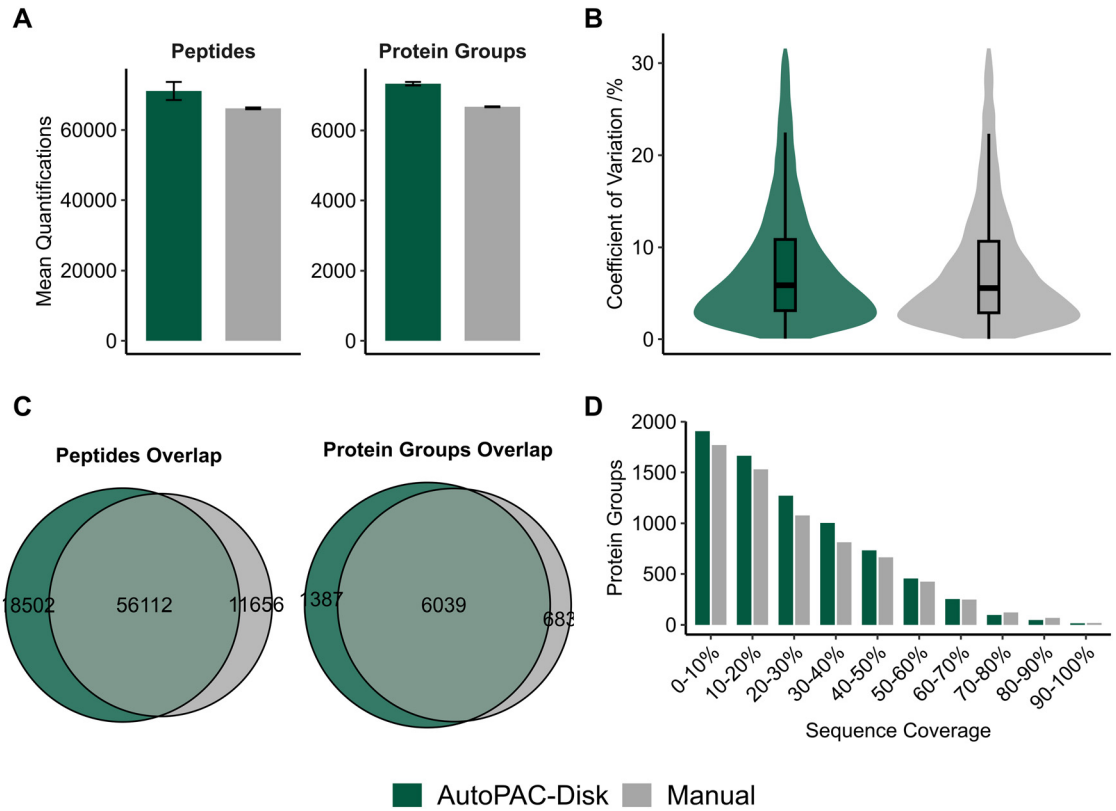

Fig. 8 Proteomic analysis of FFPE prostate tumor lysate processed using the AutoPAC-disk and a manual PAC workflow. (A) Mean of quantified peptides (left) and protein groups (right) for the AutoPAC-disk (green) and manual (grey) PAC workflow (n = 3, error bars: standard deviation). (B) Violin plots show the coefficient of variation (CV) of median normalized protein group quantities for the two workflows. The thick line represents the median, the upper and lower hinges of the boxplot represent the 25th and 75th percentiles, and the whiskers extend to ±1.5 times the interquartile range, colored as described in (A). (C) Venn diagrams show peptide (left) and protein group (right) overlaps between the two workflows, colored as described in (A). (D) Sequence coverage of unique proteins for the AutoPAC-disk and manual workflow, colored as described in (A).

Application of the AutoPAC-disk to clinically relevant FFPE prostate tumor samples

Following the initial proof-of-concept validation using HEK293 lysate, the AutoPAC-disk workflow was further evaluated using clinically relevant formalin-fixed paraffin-embedded (FFPE) prostate tumor tissue as a complex patient-derived sample matrix. The MS-based proteomic analysis of FFPE tissue samples is gaining more and more interest in the field of precision medicine and is a powerful approach to gain molecular insights beyond the capabilities of traditional histopathology.[46,47]

The FFPE block originated from a study approved by the Ethics Committee of University Medical Center Freiburg (20-1083).

Deparaffinization, lysis of FFPE sections, post-processing and nLC-MS/MS analysis followed protocols detailed in the SI (SI_methods: M4). Aliquots of 15 µg deparaffinized and lysed FFPE prostate tumor tissue (n = 3) were processed using the AutoPAC-disk and compared to the manual reference workflow. Digestion time was set to 4 hours for both workflows.

The AutoPAC-disk yielded 71 124 quantified peptides, representing a 7.5% increase compared to manual processing (66 175 peptides). On protein group level, 7336 protein groups were quantified, corresponding to a 9.9% increase over the manual workflow (6676 protein groups) (Fig. 8(A)).

Quantitative reproducibility was comparable between workflows, with protein-level CVs of 6.3% for the AutoPAC-disk and 5.9% for manual processing (Fig. 8(B)). In addition to 56 112 peptides and 6039 protein groups shared across all samples, the AutoPAC-disk yielded a larger number of exclusively identified peptides and protein groups (exclusive peptides AutoPAC-disk: 18 502, manual: 11 656; exclusive protein groups AutoPAC-disk: 1387, manual: 683) (Fig. 8(C)). Sequence coverage was generally higher for the AutoPAC-disk across a broad range of proteins, while only minor advantages for manual processing were observed at the highest coverage levels (Fig. 8(D)). Notably, the general trends observed during the detailed benchmarking with HEK293 lysates were maintained for the FFPE samples, including the absence of an apparent physicochemical identification bias and slight shift towards increased detection of lower-abundance peptides and proteins with the AutoPAC-disk.

These results demonstrate that the AutoPAC-disk workflow is compatible with clinically relevant FFPE tissue samples while maintaining robust analytical performance.

Conclusions

In this work, we present the AutoPAC-disk, a centrifugal microfluidic implementation of a PAC workflow with on-disk reagent pre-storage enabling minimal user interaction, and demonstrate assay and workflow optimizations that result in a streamlined, single-solvent PAC protocol with reduced washing steps and competitive proteomic performance. The developed system was compared against a manual reference workflow and a PAC workflow implemented on the KingFisher Apex platform using HEK293 cell lysate. This proof-of-concept study evaluated the feasibility and performance of centrifugal microfluidics for fully automated proteomic sample preparation. While all three workflows exhibited good quantitative reproducibility, the presented microfluidic approach enabled the quantification of 37 and 50% more peptides and 10 and 23% more protein groups compared to the KingFisher workflow and the manual workflow, respectively. Although the precise mechanisms underlying the increased identification rates could not be fully resolved, the additional identifications were reflected in increased sequence coverage and were predominantly associated with low-abundance proteins. Furthermore, physicochemical analysis of workflow-exclusive peptides revealed no systematic method-specific biases, supporting the robustness of the observed performance differences. The AutoPAC-disk was further applied to clinically relevant FFPE prostate tumor tissue, where it maintained the general performance trends observed in the benchmark experiments, including increased identification depth (7.5% more peptides and 9.9% more protein groups) compared to manual processing. These results demonstrate compatibility with complex clinical sample matrices and highlight the potential of the platform for future translational proteomics applications. To the best of our knowledge, the AutoPAC-disk represents the first approach to enable proteomic sample preparation for nLC-MS/MS analysis using pre-stored buffers. By minimizing bead manipulation and solvent pipetting steps, the system decreases hands-on time and operational complexity. This streamlined workflow may facilitate broader accessibility of MS-based proteomics by lowering technical barriers, particularly in laboratories with limited experience in proteomic sample preparation. The current results highlight promising potential for future use in clinical proteomic workflows, including molecular tumor boards (MTBs), where timely sample processing within a week is required.[5]

Author contributions

These authors contributed equally. Michelle Hinrichs: conceptualization, methodology, investigation: developed the centrifugal microfluidic implementation, established automated PAC processing on the AutoPAC-disk, and conducted the manual and on-disk sample preparations for benchmarking and provided ideas for the data analysis, visualization, formal analysis, writing – original draft. Johanna Wallner: conceptualization, methodology, investigation: performed the main data analysis and visualization of the nLC-MS/MS data, all workflow adaptation and semi-automated experiments, and nLC-MS/MS measurements, visualization, formal analysis, writing – original draft. Johanna Thiery: resources, writing – review. Carolin Kleber: investigation, writing – review & editing. Manuel Metzger: investigation, writing – review. Stephan A. Sieber: supervision, writing – review & editing. Tobias Hutzenlaub: supervision, funding acquisition, writing – review & editing. Oliver Schilling: conceptualization, writing – review & editing. Nils Paust: supervision, writing – review & editing. Hannes Hahne: supervision, project administration, writing – review & editing. Jan Muntel: conceptualization, supervision, writing – review & editing. Jan-Niklas Klatt: conceptualization, supervision, project administration, writing – review & editing.

Conflicts of interest

The authors declare the following competing financial interest(s): competing financial interests: the authors JW, JM, and HH are full-time employees of OmicScouts, a Momentum Biotechnology Company.

Data availability

The mass spectrometry proteomics data have been deposited to the ProteomeXchange Consortium *via* the PRIDE[48] partner repository with the dataset identifier PXD072920.

Supplementary information (SI): SI1: lists all materials and chemicals used in this manuscript (xlsx). SI_methods: includes the description of cell culturing and cell lysis, describing the standard workflow of the robotic sample preparation for manual protocol development experiments (bead testing, organic solvent testing, stick pack experiment), and methods for FFPE experiment (docx). SI_results: detail the results for the manual protocol development experiments (bead testing, organic solvent testing), the microfluidic protocol, additional information about the bead column chamber, and the comparative performance of PAC workflows (docx). See DOI: https://doi.org/10.1039/d6lc00211k.

Acknowledgements

Financial support by the Bundesministerium für Forschung, Technologie und Raumfahrt within the project ESTHER (FKZ - 13GW0603D, 13GW0603A, 13GW0603E) is gratefully acknowledged. Manuscript editing was supported by Perplexity (Perplexity AI) and GPT-5.1 (OpenAI). All original content was authored by the authors themselves, who reviewed, edited, and approved all AI-assisted outputs. The authors take full responsibility for the final content of the

published article. Data analysis scripts (R) were improved with assistance from ChatGPT (OpenAI).

Notes and references

1 N. A. Brown and K. S. J. Elenitoba-Johnson, *Annu. Rev. Pathol.: Mech. Dis.*, 2020, **15**, 97–121, DOI: 10.1146/annurev-pathmechdis-012418-012735.

2 S. Beg, R. Bareja, K. Ohara, K. W. Eng, D. C. Wilkes, D. J. Pisapia, W. A. Zoughbi, S. Kudman, W. Zhang, R. Rao, J. Manohar, T. Kane, M. Sigouros, J. Z. Xiang, F. Khani, B. D. Robinson, B. M. Faltas, C. N. Sternberg, A. Sboner, H. Beltran, O. Elemento and J. M. Mosquera, *Transl. Oncol.*, 2021, **14**, 100944, DOI: 10.1016/j.tranon.2020.100944.

3 J. R. Lill, W. R. Mathews, C. M. Rose and M. Schirle, *Expert Rev. Proteomics*, 2021, **18**, 503–526, DOI: 10.1080/14789450.2021.1962300.

4 A. W. S. Fung, V. Sugumar, A. H. Ren and V. Kulasingam, *J. Clin. Pathol.*, 2020, **73**, 61–69, DOI: 10.1136/jclinpath-2019-206269.

5 J. Thiery and M. Fahrner, *Proteomics*, 2024, **24**, 2300002, DOI: 10.1002/pmic.202300002.

6 D. V. Miller, K. N. Bhatt, G. T. Bocsi, A. Chang, P. P. Gopal, M. Hernandez, T. Kalicanin, E. D. McPhail, M. O. Nakashima, M. M. Picken, L. Souter, V. F. Torous, A. J. Zemek and B. S. Fyfe, *Arch. Pathol. Lab. Med.*, 2025, **150**(3), 179–193, DOI: 10.5858/arpa.2025-0275-CP.

7 E. M. McCormick, *Genome Med.*, 2025, **17**, 61, DOI: 10.1186/s13073-025-01491-z.

8 Y. Jiang, D. A. B. Rex, D. Schuster, B. A. Neely, G. L. Rosano, N. Volkmar, A. Momenzadeh, T. M. Peters-Clarke, S. B. Egbert, S. Kreimer, E. H. Doud, O. M. Crook, A. K. Yadav, M. Vanuopadath, A. D. Hegeman, M. L. Mayta, A. G. Duboff, N. M. Riley, R. L. Moritz and J. G. Meyer, *ACS Meas. Sci. Au*, 2024, **4**, 338–417, DOI: 10.1021/acsmeasuresciau.3c00068.

9 R. Aebersold and M. Mann, *Nature*, 2003, **422**, 198–207, DOI: 10.1038/nature01511.

10 R. Aebersold and M. Mann, *Nature*, 2016, **537**, 347–355, DOI: 10.1038/nature19949.

11 V.-A. Duong and H. Lee, *Int. J. Mol. Sci.*, 2023, **24**, 5350, DOI: 10.3390/ ijms24065350.

12 A. G. Birhanu, *Clin. Proteomics*, 2023, **20**, 32, DOI: 10.1186/s12014-023-09424-x.

13 C. S. Hughes, S. Foehr, D. A. Garfield, E. E. Furlong, L. M. Steinmetz and J. Krijgsveld, *Mol. Syst. Biol.*, 2014, **10**, 757, DOI: 10.15252/msb.20145625.

14 C. S. Hughes, S. Moggridge, T. Müller, P. H. Sorensen, G. B. Morin and J. Krijgsveld, *Nat. Protoc.*, 2019, **14**, 68–85, DOI: 10.1038/s41596-018-0082-x.

15 H. E. Johnston, K. Yadav, J. M. Kirkpatrick, G. S. Biggs, D. Oxley, H. B. Kramer and R. S. Samant, *Anal. Chem.*, 2022, **94**, 10320–10328, DOI: 10.1021/acs.analchem.1c04200.

16 T. S. Batth, M. X. Tollenaere, P. Rüther, A. Gonzalez-Franquesa, B. S. Prabhakar, S. Bekker-Jensen, A. S. Deshmukh and J. V. Olsen, *Mol. Cell. Proteomics*, 2019, **18**, 1027–1035, DOI: 10.1074/mcp.TIR118.001270.

17 M. Leutert, R. A. Rodríguez-Mias, N. K. Fukuda and J. Villén, *Mol. Syst. Biol.*, 2019, **15**, e9021, DOI: 10.15252/msb.20199021.

18 T. Müller, M. Kalxdorf, R. Longuespée, D. N. Kazdal, A. Stenzinger and J. Krijgsveld, *Mol. Syst. Biol.*, 2020, **16**, e9111, DOI: 10.15252/msb.20199111.

19 M. Tang, G. Wang, S.-K. Kong and H.-P. Ho, *Micromachines*, 2016, **7**, 26, DOI: 10.3390/mi7020026.

20 P. Juelg, E. Kipf, M. Specht, M. Fillies, C. Eckert, N. Paust, R. Zengerle, M. Lehnert and T. Hutzenlaub, *Lab Chip*, 2021, **21**, 558–570, DOI: 10.1039/D0LC00945H.

21 J. F. Hess, M. E. Hess, R. Zengerle, N. Paust, M. Boerries and T. Hutzenlaub, *Anal. Chim. Acta*, 2021, **1182**, 338954, DOI: 10.1016/j.aca.2021.338954.

22 J.-N. Klatt, M. Depke, N. Goswami, N. Paust, R. Zengerle, F. Schmidt and T. Hutzenlaub, *Lab Chip*, 2020, **20**, 2937–2946, DOI: 10.1039/D0LC00530D.

23 J.-N. Klatt, T. J. Dinh, O. Schilling, R. Zengerle, F. Schmidt, T. Hutzenlaub and N. Paust, *Lab Chip*, 2021, **21**, 2255–2264, DOI: 10.1039/D1LC00137J.

24 J. Peng, C. Chan, S. Zhang, A. A. Sklavounos, M. E. Olson, E. Y. Scott, Y. Hu, V. Rajesh, B. B. Li, M. D. Chamberlain, S. Zhang, H. Peng and A. R. Wheeler, *Chem. Sci.*, 2023, **14**, 2887–2900, DOI: 10.1039/d3sc00560g.

25 M. K. Steinbach, J. Leipert, T. Matzanke and A. Tholey, *Small Methods*, 2025, **9**, 2400495, DOI: 10.1002/smtd.202400495.

26 J. Leipert and A. Tholey, *Lab Chip*, 2019, **19**, 3490–3498, DOI: 10.1039/C9LC00715F.

27 Y. Zhu, P. D. Piehowski, R. Zhao, J. Chen, Y. Shen, R. J. Moore, A. K. Shukla, V. A. Petyuk, M. Campbell-Thompson, C. E. Mathews, R. D. Smith, W.-J. Qian and R. T. Kelly, *Nat. Commun.*, 2018, **9**, 882, DOI: 10.1038/s41467-018-03367-w.

28 I. Schwarz, S. Zehnle, T. Hutzenlaub, R. Zengerle and N. Paust, *Lab Chip*, 2016, **16**, 1873–1885, DOI: 10.1039/C5LC01525A.

29 M. Focke, F. Stumpf, B. Faltin, P. Reith, D. Bamarni, S. Wadle, C. Müller, H. Reinecke, J. Schrenzel, P. Francois, D. Mark, G. Roth, R. Zengerle and F. Von Stetten, *Lab Chip*, 2010, **10**, 2519–2526, DOI: 10.1039/C004954A.

30 J. Schlanderer, H. Hoffmann, J. Lüddecke, A. Golubov, W. Grasse, E. V. Kindler, T. A. Kohl, M. Merker, C. Metzger, V. Mohr, S. Niemann, C. Pilloni, S. Plesnik, B. Raya, B. Shresta, C. Utpatel, R. Zengerle, M. Beutler and N. Paust, *Lab Chip*, 2024, **24**, 74–84, DOI: 10.1039/d3lc00783a.

31 J. Rappsilber, M. Mann and Y. Ishihama, *Nat. Protoc.*, 2007, **2**, 1896–1906, DOI: 10.1038/nprot.2007.261.

32 M. C. Chambers, B. Maclean, R. Burke, D. Amodei, D. L. Ruderman, S. Neumann, L. Gatto, B. Fischer, B. Pratt, J. Egertson, K. Hoff, D. Kessner, N. Tasman, N. Shulman, B. Frewen, T. A. Baker, M.-Y. Brusniak, C. Paulse, D. Creasy, L. Flashner, K. Kani, C. Moulding, S. L. Seymour, L. M. Nuwaysir, B. Lefebvre, F. Kuhlmann, J. Roark, P. Rainer, S. Detlev, T. Hemenway, A. Huhmer, J. Langridge, B. Connolly, T. Chadick, K. Holly, J. Eckels, E. W. Deutsch, R. L. Moritz, J. E. Katz, D. B. Agus, M. MacCoss, D. L. Tabb and P. Mallick, *Nat. Biotechnol.*, 2012, **30**, 918–920, DOI: 10.1038/nbt.2377.

33 A. T. Kong, F. V. Leprevost, D. M. Avtonomov, D. Mellacheruvu and A. I. Nesvizhskii, *Nat. Methods*, 2017, **14**, 513–520, DOI: 10.1038/nmeth.4256.
34 V. Demichev, C. B. Messner, S. I. Vernardis, K. S. Lilley and M. Ralser, *Nat. Methods*, 2020, **17**, 41–44, DOI: 10.1038/s41592-019-0638-x.
35 R Core Team, 2024.
36 Posit team, *Posit Software, PBC*.
37 H. Wickham, *ggplot2: Elegant Graphics for Data Analysis*, Springer-Verlag, New York, 2016.
38 D. Osorio, P. Rondon-Villarreal and R. Torres, Peptides: A package for data mining of antimicrobial peptides, *The R Journal*, 2015, **7**(1), 4–14, DOI: 10.32614/CRAN.package.Peptides.
39 Proteomics Unit at University of Bergen, SP3, Single-pot, solid-phase-enhanced sample Preparation, https://www.uib.no/sites/w3.uib.no/files/attachments/sp3_protein_digestion_protocol.pdf.
40 O. Strohmeier, M. Keller, F. Schwemmer, S. Zehnle, D. Mark, F. Von Stetten, R. Zengerle and N. Paust, *Chem. Soc. Rev.*, 2015, **44**, 6187–6229, DOI: 10.1039/c4cs00371c.
41 S. Zehnle, F. Schwemmer, G. Roth, F. Von Stetten, R. Zengerle and N. Paust, *Lab Chip*, 2012, **12**, 5142, DOI: 10.1039/c2lc40942a.
42 J. F. Hess, S. Zehnle, P. Juelg, T. Hutzenlaub, R. Zengerle and N. Paust, *Lab Chip*, 2019, **19**, 3745–3770, DOI: 10.1039/C9LC00441F.
43 T. Van Oordt, Y. Barb, J. Smetana, R. Zengerle and F. Von Stetten, *Lab Chip*, 2013, **13**, 2888, DOI: 10.1039/C3LC50404B.
44 M. Grumann, A. Geipel, L. Riegger, R. Zengerle and J. Ducrée, *Lab Chip*, 2005, **5**, 560, DOI: 10.1039/B418253G.
45 T. Müller, M. Kalxdorf, R. Longuespée, D. N. Kazdal, A. Stenzinger and J. Krijgsveld, *Mol. Syst. Biol.*, 2020, **16**, DOI: 10.15252/msb.20199111.
46 F. Coscia, S. Doll, J. M. Bech, L. Schweizer, A. Mund, E. Lengyel, J. Lindebjerg, G. I. Madsen, J. M. Moreira and M. Mann, *J. Pathol.*, 2020, **251**, 100–112, DOI: 10.1002/path.5420.
47 S. A. AlHammadi, L. N. Nagshabandi, H. Muhammad, H. H. Sukkarieh and A. Aljada, *Clin. Proteomics*, 2025, **22**, 45, DOI: 10.1186/s12014-025-09567-z.
48 Y. Perez-Riverol, C. Bandla, D. J. Kundu, S. Kamatchinathan, J. Bai, S. Hewapathirana, N. S. John, A. Prakash, M. Walzer, S. Wang and J. A. Vizcaíno, *Nucleic Acids Res.*, 2025, **53**, D543–D553, DOI: 10.1093/nar/gkae1011.

